Effects of Surface Topography and Cellular Biomechanics on Nanopillar-Induced Bactericidal Activity

Amin Valiei, Jean-François Bryche, Michael Canva, Paul G Charette, Christopher Moraes, Reghan J Hill, Nathalie Tufenkji

Effects of surface topography and cellular biomechanics on nanopillar-induced bactericidal activity

Amin Valiei[1*], Jean-François Bryche[2,3], Michael Canva[2,3], Paul G. Charette[2,3], Christopher Moraes[1,4,5], Reghan J. Hill[1*], and Nathalie Tufenkji[1]

[1]Department of Chemical Engineering, McGill University, Montreal, Québec H3A 0C5, Canada.

[2]Laboratoire Nanotechnologies Nanosystèmes (LN2)-IRL3463, CNRS, Université de Sherbrooke, Université Grenoble Alpes, École Centrale de Lyon, INSA Lyon, Sherbrooke, Québec J1K 0A5, Canada

[3]Institut Interdisciplinaire d'Innovation Technologique (3IT), Université de Sherbrooke, 3000 Boulevard de l'Université, Sherbrooke, Québec J1K OA5, Canada.

[4]Department of Biomedical Engineering, McGill University, Montreal, Québec H3A 0C5, Canada

[5]Goodman Cancer Research Center, McGill University, Montreal, Québec H3A 0G4, Canada.

*Corresponding authors: amin.valiei@mail.mcgill.ca, reghan.hill@mcgill.ca

ABSTRACT: Bacteria are mechanically resistant biological structures that can sustain physical stress. Experimental data, however, have shown that high-aspect-ratio nanopillars deform bacterial cells upon contact. If the deformation is sufficiently large, it lyses the bacterial cell wall, ultimately leading to cell death. This has prompted a novel strategy, known as mechano-bactericide technology, to fabricate antibacterial surfaces. Although adhesion forces were originally proposed as the driving force for mechano-bactericidal action, it has been recently shown that external forces, such as capillary forces arising from an air−water interface at bacterial surfaces, produce sufficient loads to rapidly kill bacteria on nanopillars. This discovery highlights the need to theoretically examine how bacteria respond to external loads and to ascertain the key factors. In this study, we developed a finite element model approximating bacteria as elastic shells filled with cytoplasmic fluid brought into contact with an individual nanopillar or nanopillar array. This model elucidates that bacterial killing caused by external forces on nanopillars is influenced by surface topography and cell biomechanical variables, including the density and arrangement of nanopillars, in addition to the cell wall thickness and elastic modulus. Considering that surface topography is an important design parameter, we performed experiments using nanopillar arrays with precisely controlled nanopillar diameters and spacing. Consistent with model predictions, these demonstrate that nanopillars with a larger spacing increase bacterial susceptibility to mechanical puncture. The results provide salient insights into mechano-bactericidal activity and identify key design parameters for implementing this technology.

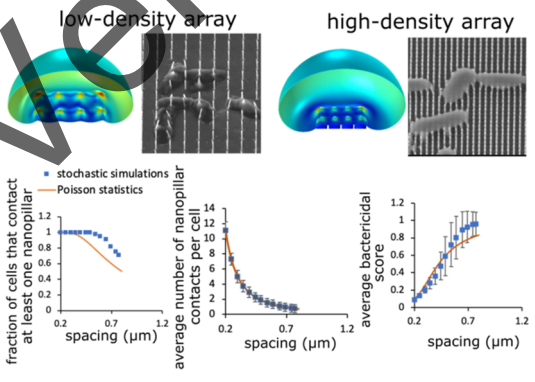

KEYWORDS: *antibacterial surfaces, nanopillar arrays, contact mechanics, cell rigidity, antimicrobial material*

INTRODUCTION

In recent years, surfaces textured with nanopillars have gained attention for their antibacterial properties.[1−3] Presenting an array of nanopillars with diameters smaller than bacterial dimensions, these surfaces mechanically deform bacteria upon contact.[1−5] If the deformations are large enough, they permanently damage the cell membrane, causing cell lysis.[1,2,6] Since this antibacterial mechanism deploys physical forces instead of chemical interactions (e.g., antibiotics or disinfectants) to kill bacteria, it reduces the likelihood of antibiotic resistance and eliminates the release of toxic chemicals.[2,7] Therefore, it is considered a robust and sustainable alternative antibacterial strategy.[2,7] Nanopillar-textured surfaces, by their unique potential to tackle the bacterial chemical-resistance problem, offer a new perspective for developing antibacterial materials for industrial antifouling surfaces, environmental surfaces in healthcare settings, and medical implants.[2,8,9] The success of this technology depends, in part, on the fabrication of nanopillars for a diverse range of substrates and the establishment of appropriate environmental conditions for maximizing their effect.[1,2]

Accordingly, understanding and optimizing the effect are essential for technological applications.

In a previous work, we showed that external mechanical forces are essential elements for killing bacteria on nanopillared surfaces.[9] While, conventionally, bacterial adhesion forces were considered as the main driving force for deforming bacteria on nanopillars,[10,11] we observed that bacteria on silicon and ZnO nanopillars remained viable during long assay periods when the substrates were fully immersed.[9,11] This suggests that adhesion alone is insufficient to cause rapid cell death.[9,11] When bacteria on nanopillars were exposed to either capillary forces of an air/liquid interface or reaction forces from an external weight, they were structurally damaged and rapidly killed.[9,11] Thus, harnessing external forces to reduce the action time offers a

novel means of improving the mechano-bactericidal effect, paving the way for new applications, such as environmental antibacterial surfaces. For instance, the air−liquid interface formed during evaporation can effectively eliminate bacteria from contaminated droplets (e.g., respiratory droplets) or intermittent liquid contact (e.g., cleaning the surfaces of medical equipment).[11]

Given the importance of this discovery, there is a need to better understand the mechanism of bacterial killing on nanopillars. Since adhesion was considered the dominant mechanism for bacterial killing, many theoretical models have been developed to help explain the mechanism.[12−15] In these models, insights into the mechano-bactericidal effect were obtained by minimizing the free energy of adhesion and mechanical deformation.[13−15] For example, in one of the pioneering models, Pogodin et al. predicted that in the mechano-bactericidal effects driven by adhesion, nanopillars do not directly puncture a cell, but stretching and rupture of the cell wall in the nanopillar interspacing area is the main cause of cell rupture.[13] These approaches have been of great interest to elucidate bacterial deformation caused by adhesion effects; however, further modeling efforts are required to address this mechanism when external forces, such as those caused by capillarity, are the dominant drivers.

To help assess simplifying approximations in the analytical models, more direct modeling approaches, such as finite element analysis (FEA) have been recently adopted. The FEA approach allows for resolving localized stress and strain fields, providing a different and arguably more realistic illustration of the interactions between nanopillars and cells. Velic et al.[16] and Cui et al.[17] developed FEA models to study bacterial killing on nanopillars caused by adhesion forces between the cell wall and nanopillars. Using this approach, the authors calculated the stress field developed on the cell wall, which was further used to estimate the adhesion energies required to cause cell wall rupture. In another work, Mirzaali et al.[18] computed the cell deformation on nanopillars caused by the weight of the bacterial cell and the surrounding liquid. More recently, Islam et al. modeled the mechanism of bacteria−nanopillar mechanical interaction, elucidating the formation of concentrated stress rings and cell wall puncture.[19] Furthermore, FEA models have been used to determine the optimal substrate fabrication parameters. These investigations led to different trends, stemming from the problem formulations and assumptions (see Table S1). In terms of the interpillar spacing, for instance, Cui et al. reported a significant impact on adhesion forces and cell wall stress, identifying an optimum spacing value at ~175 nm.[17] Valic et al. found a weak correlation between nanopillar spacing and cell deformation, obtaining an optimum spacing of 125 nm.[16] Mirzaali et al. argued in favor of larger spacings and proposed an optimal spacing of 300 nm.[18] Overall, the assessment of previous FEA models highlights the immense benefits of FEA for conducting rigorous case studies. However, as each of the past works is based on a specific type of force and class of bacterial strain, a broad picture of the biomechanical and topographical effects on the mechano-bactericidal effect is lacking.

In this work, we provide new insights into mechano-bactericidal mechanisms by introducing an FEA model that has three distinctive features. (i) Being inspired by our recent experimental work highlighting the primary role of external forces (such as capillarity) in mechano-bactericidal effects, our model aims to simulate bacterial deformation under non-specific external loads. This unexplored domain is pertinent to bacterial deformation under both body and surface forces that can serve as indentation loads. This would be essential for comparing and reconciling results from various mechanisms. (ii) The model presents an integrative accounting of cell biomechanical effects, including the variation of the internal cell pressure (turgor) during the deformation, which is missing in earlier FEA models. This inclusion can increase the accuracy of the simulation, according to Cui et al.'s findings.[17] (iii) It provides a systematic and comprehensive analysis of key biomechanical parameters and nanopillar arrangement, which suggests the relevance of the findings to a broad range of problems. Through this model, we demonstrate that cell wall properties and nanopillar configuration are critical parameters that can substantially impact the potency of mechano-bactericidal activity. We also identify optimal nanopillar design parameters for maximizing mechano-bactericidal killing. Motivated by the theoretical results, we performed mechano-bactericidal experiments using nanopillar arrays of controlled size and arrangement. Realizing a strong concordance between experimental data and modeling outcomes, we conclude that both approaches, when used hand-in-hand, are beneficial for guiding the design of functional antibacterial materials.

MATERIALS AND METHODS

Model Formulation. Numerical simulations of a bacterium deformation on nanopillars were performed using the Structural Mechanics Module of COMSOL Multiphysics v.5.5 (Comsol Inc., USA) in 2D-axisymmetric and 3D geometries.

Geometry. The geometry of the base model comprises a spherical bacterium with an outer diameter of 500 nm and an inner diameter of 495 nm (cell wall thickness 2.5 nm,[20] corresponding to the wall thickness of Gram-negative *Pseudomonas aeruginosa*). For the Gram-positive bacterium, the cell dimensions mimic *Staphylococcus aureus* with an outer diameter of 500 nm and inner diameter of 450 nm (cell wall thickness = 25 nm[21]). The nanopillar diameter is taken to be 50 nm as a representative size of bactericidal nanopillars and based on the diameter of silicon nanopillars exhibiting a high kill efficacy (~99.9% for *Pseudomonas aeruginosa*).[9]

Physical Properties. A bacterium is modeled as an elastic shell with physical properties representative of a typical bacterial cell envelope. The cell envelope of Gram-negative bacteria comprises an inner and outer membrane sandwiching a peptidoglycan layer.[22] The cell envelope of Gram-positive bacteria comprises a peptidoglycan layer and an inner membrane.[22] It is well established that the mechanical stiffness of a bacterial cell relies primarily on the rigid peptidoglycan layer.[23] For simplicity, the elastic shell was assumed to be homogeneous and isotropic, reflecting the elastic properties of the peptidoglycan layer (also termed the cell wall).[23] For the base model, we assumed an elastic modulus of 30 MPa[24] (refer to Table 1 in the review article by Elbourne et al.[25] for the range of relevant values), Poisson ratio of 0.3,[26] a yield strength of 13 MPa for the cell wall, based on published estimates,[24] and an internal hydrostatic pressure of 0.3 bar, a value measured directly by atomic force microscopy.[27] When the model was executed at the cell wall elastic modulus of 200 MPa to study the effect of bacterial stiffness, a yield strength of 90 MPa corresponding to 45% breaking strain was used, identical to the assumption of Cui et al.[17] and in agreement with Thwaites' measurements.[24] The nanopillars were modeled as silicon with an elastic modulus of 130 GPa.[28] All materials were approximated as linearly elastic.

Boundary Conditions. A contact boundary condition between the lower surface of the elastic shell and the nanopillar was specified (penalty-factor method), and a vertical displacement toward the nanopillar was prescribed for the apical point of the top shell surface. This equates the problem to bacterial deformation under body force or a surface load with a negligible impact on the contact region. The

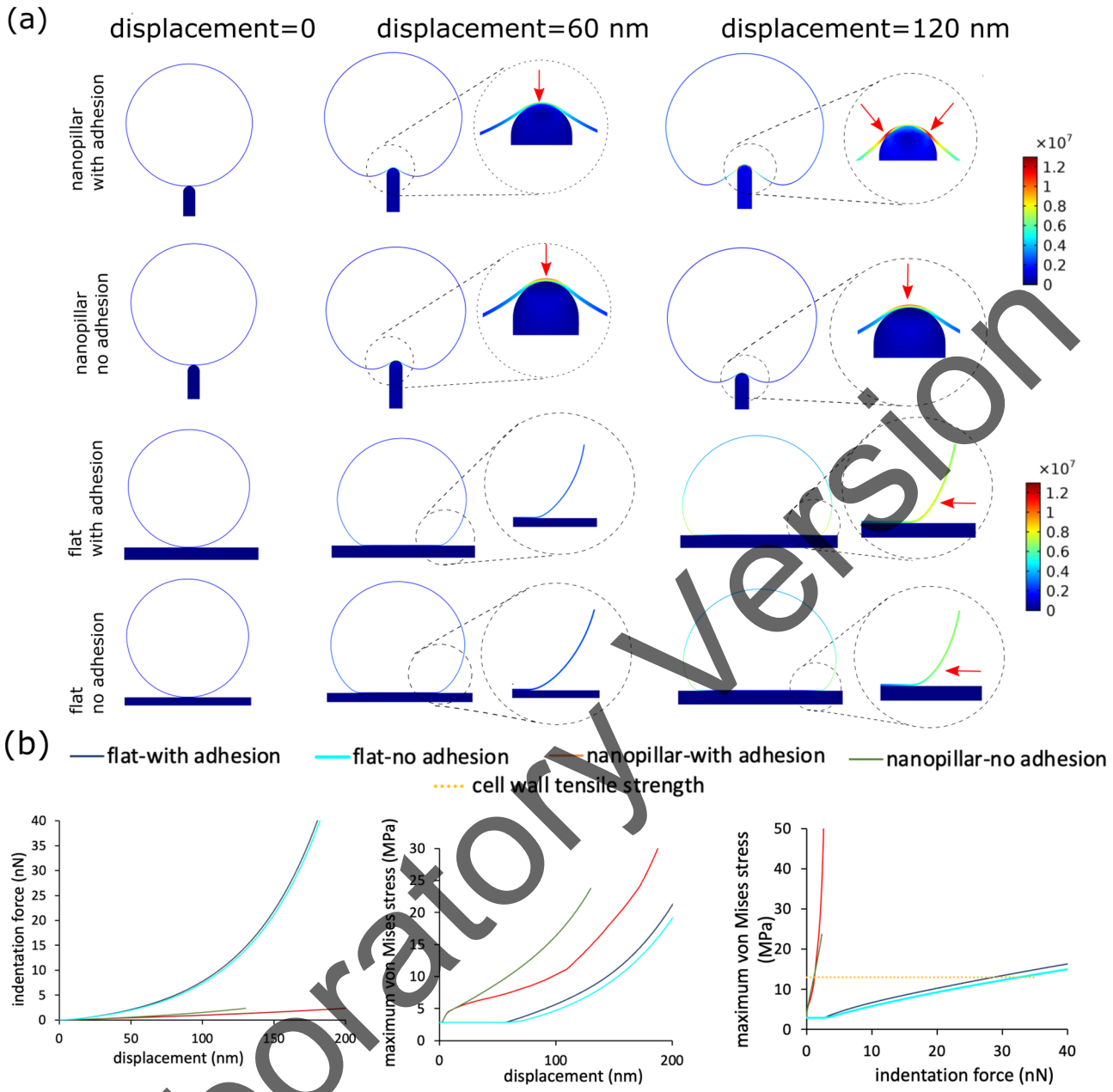

Figure 1. Bacterial deformation on a flat surface and a single nanopillar under an external load. (a) Shape profiles as a function of the vertical downward displacement of bacteria with and without adhesion. Red arrows identify the locations of maximum stress. All of the cell profiles are to scale. (b) Indentation force versus displacement, maximum von Mises stress versus displacement, and maximum von Mises stress versus indentation force. The yellow dashed line shows the approximated value of the cell wall tensile strength.

adhesion condition concerns the geometrical attachment of engaging surfaces upon contact and does not involve any quantitative definition of molecular adhesion forces such as van der Waals forces. The bacterial deformation was evaluated in adhesion mode for all models, except when adhesion and nonadhesion modes were compared in which case the adhesion assumption is explicitly noted. A uniform pressure boundary condition was assigned to the internal surfaces of the bacterial shell. Given the incompressibility of the liquid cell cytoplasm, we defined a constant internal volume constraint for the elastic shell. Accordingly, for each indentation step, the internal pressure is automatically adjusted to satisfy this constraint.

Mesh. For 2D simulations, a quadrilateral mesh with a maximum element size of 1 nm was used on the bacterial envelope, and a triangular mesh with a maximum element size of 2 nm was used for the nanopillar. The bacterial cell wall mesh comprised 2369 elements, and the nanopillar was comprised of 1159 elements. For 3D simulations, a free triangular mesh with maximum element size 1 nm was prescribed across the shell thickness and maximum element size 2 nm prescribed on the nanopillars. For the bacterial cell wall, the mesh was revolved along the bacterial quarter sphere to create a swept mesh with 50 elements. The bacterial cell wall comprised 705,550 tetrahedral elements and each nanopillar 10,601 elements. All of the mesh sizes were chosen according to an appropriate mesh independence study.

Solution. Bacterial indentation was implemented by using the auxiliary sweep option of the stationary solver to model the cell displacement (1 nm increments). Total contact force and von Mises stress values were calculated from the solution.

EXPERIMENTAL SECTION

Ordered Nanopillar Array Fabrication. E-beam lithography was used to fabricate ordered nanopillars with two different diameters

and several different spacings (diameter = 90 nm, spacing = 200, 300, 400, and 600 nm; diameter = 200 nm, spacing = 300, 400, and 600 nm). First, silicon wafers (Pure Wafer, USA) were cleaned thoroughly with three successive 5 min baths of propan-2-one, propan-2-ol, and deionized water. Then, a negative resist layer of Ma-N 2401 (Kayaku Advanced Materials, USA) was spin-coated on the substrate with the adhesion promoter hexamethyldisilazane (HMDS, Sigma-Aldrich, Canada). The total thickness of the resist is 500 nm. The fabrication parameters were varied in the lithography, using a modified Zeiss microscope (Leo 1540 XB, Zeiss, Germany), to produce designs with the desired diameter, density, and periodicity. Following lithographic exposure, wafers were developed in a solution of Ma-D 525 (MicroChem Corp, USA). Thereafter, an etching process was carried out at a rate adjusted based on the intended pillar height (~100 nm/min), in a mixture of sulfur hexafluoride and octafluorocyclobutane, in an inductively coupled plasma etching system at 20 °C. Following the fabrication, wafers were cleaned by removing the photoresist residues through rinsing in Remover1165 (Dow Chemical Company, USA) and O_2 plasma cleaner (Plasmaline 415, Tegal, USA).

Preparation of Bacterial Culture. The bacterial strain *P. aeruginosa* (PAO1), a widely used model of Gram-negative pathogenic bacteria, was used in the experiments.[29] The bacterial source was preserved in −80 °C glycerol stocks, from which fresh cultures were streaked onto a Luria−Bertani (LB, Life Technologies, USA) agar plate before each experiment. Bacterial suspensions were prepared by first transferring a single colony from agar plates to the LB liquid medium (5 mL) and then incubating overnight at 37 °C until reaching a logarithmic growth phase. The final working suspensions were obtained by centrifuging the overnight culture (3000*g* for 4 min) and resuspending the bacterial pellets in physiological phosphate-buffered saline. The bacteria concentration was adjusted before each experiment by ensuring an optical density (OD_{600}) of ~0.3, measured via a UV−visible spectrophotometer (Biomate 3S, Thermo Scientific, USA).

Scanning Electron Microscopy (SEM) Analysis. To evaluate the morphology of attached bacteria upon mechano-bactericidal activity induced by capillary forces, nanopillared samples were fully submerged in bacterial suspension (2 mL) in 12-well microtiter plates (Corning Incorporated, USA). Upon a 30 min waiting time, sufficient to ensure bacterial attachment, samples were exposed to ambient air under sterile conditions allowing the liquid to evaporate (~20 min, T = 21 °C, relative humidity (RH) ~20−40%). Immediately following evaporation, bacteria were fixed by gently placing 2.5% glutaraldehyde over the substrates and then incubated overnight at 4 °C. To avoid artifacts upon exposure of bacteria to vacuum during SEM, critical-point drying was adopted. First, the liquid inside the well plates was replaced with ethanol through a stepwise increase of ethanol concentration (30, 50, 70, 80, 90, 100, 100 and 100%), over waiting intervals of 10 min. Next, in a critical-point dryer (EM CPD030, Leica Microsystems, Germany), ethanol covering the samples was replaced with CO_2, which was then discharged at the supercritical fluid state. Samples were then imaged at a 5 kV acceleration voltage by using SEM (FEI Inspect F50 FE-SEM, FEI Company, USA).

RESULTS AND DISCUSSION

Bacterial Deformation on a Flat Surface and on a Nanopillar. The central aspect of the mechano-bactericidal mechanism, which is known to typically appear on high-aspect-ratio nanopillars, is surface topography. To build representative models of mechano-bactericidal activity, we first characterized cellular deformation on a nanopillar, as the basic mechano-bactericide unit, comparing it with the bacterial mechanical interaction with a flat surface. We modeled the deformation of a typical Gram-negative bacterium (with the biophysical parameters matching those of *Pseudomonas aeruginosa*) under a linear displacement. The nanopillar geometry comprised a single pillar with diameter D = 50 nm, similar to the dimension of etched silicon nanopillars used in previous studies and known to cause a substantial bactericidal effect.[9] The von Mises failure criterion, which relates the calculated stress to the yield strength measured in a uniaxial tensile test, was adopted to assess the yield criteria, similar to previous models[17,30] and other biomechanical studies.[31] The model was implemented with and without adhesive contact between the bacterial cell wall and nanopillars.

The force and stress characteristics of a bacterial cell wall pressing against the substrates mentioned above are illustrated in Figure 1. The cell in the reference condition is under mild stress of the internal cell pressure, which, as expected, is considerably below (31%) the yield strength. Upon the cell pressing against the nanopillar, considerable stress develops at the point of contact (Figure 1a), as indicated by the force and stress versus displacement and force versus von Mises stress curves (Figure 1b). The simulation shows that a substantially smaller force (1.2 nN under adhesion, and 0.9 nN for nonadhesion contact) is required to yield bacteria on the nanopillar than on the flat surface (25.2 nN under adhesion condition, 26.4 nN for nonadhesion). Accounting for the difference in reported values of cell elastic modulus, which range from 30 to 200 MPa,[25] the range of indentation forces (1−7 nN) resulting in cell wall yield on nanopillars, termed yield forces, is consistent with values from indentation experiments (a detailed discussion on the role of cell biomechanics is provided in the next section). Examples of reported puncture forces include 1−2 nN by Suo et al.,[32] 10 nN by Liu et al.,[33] and 20 nN by del Valle et al.[34]

Bacteria adhering to surfaces may experience various forces, including adhesion forces, which are typically estimated to be less than 1 nN or at most a few nN,[25] as well as gravitational forces with much smaller magnitude (10^{-3} nN). Additionally, when bacteria transition from their natural wet environments to dry surfaces, capillary forces come into play from liquid evaporation. These capillary forces can become significant, reaching magnitudes of several tens to hundreds of nN when the surfaces are sufficiently hydrophilic,[11] far surpassing adhesion and gravitational forces.[9] The experimentally observed bactericidal destruction by capillary forces on nanopillars can thus be attributed to the much higher value of these forces compared with the predicted cell wall yield forces (on these topographies). Conversely, consistent with simulations indicating that bacteria are considerably more resistant to deformation and yielding on flat surfaces, capillary forces result in negligible bacterial deformation on smooth surfaces.[9,11] Also consistent with our experimental observations,[9] other forces, such as adhesion forces, which are typically smaller than the yield forces, have negligible effects on bacterial morphology when on flat and nanopillar topographies.

From a mechanistic perspective, the stress calculated by the model allows for further analysis of bacterial deformation and potential rupture, particularly in the context of the existing debate on the location of cellular disintegration. Pogodin et al. postulated that the strong adhesion of bacteria to nanopillars produces excessive stretching of the suspending cell wall, and that the tension from this deformation leads to a cell wall fracture with no puncturing.[13] Velic et al.[16] and Islam et al.,[19] in contrast, predicted a different response, suggesting a local increase in the stress on nanopillars. In our comparative model, we see that although on a flat surface the stress has a much more uniform distribution, the stress concentrates focally on a nanopillar in the form of a central spot (without adhesion) or a ring (with adhesion) (Figure 1a, red arrows). Previous studies

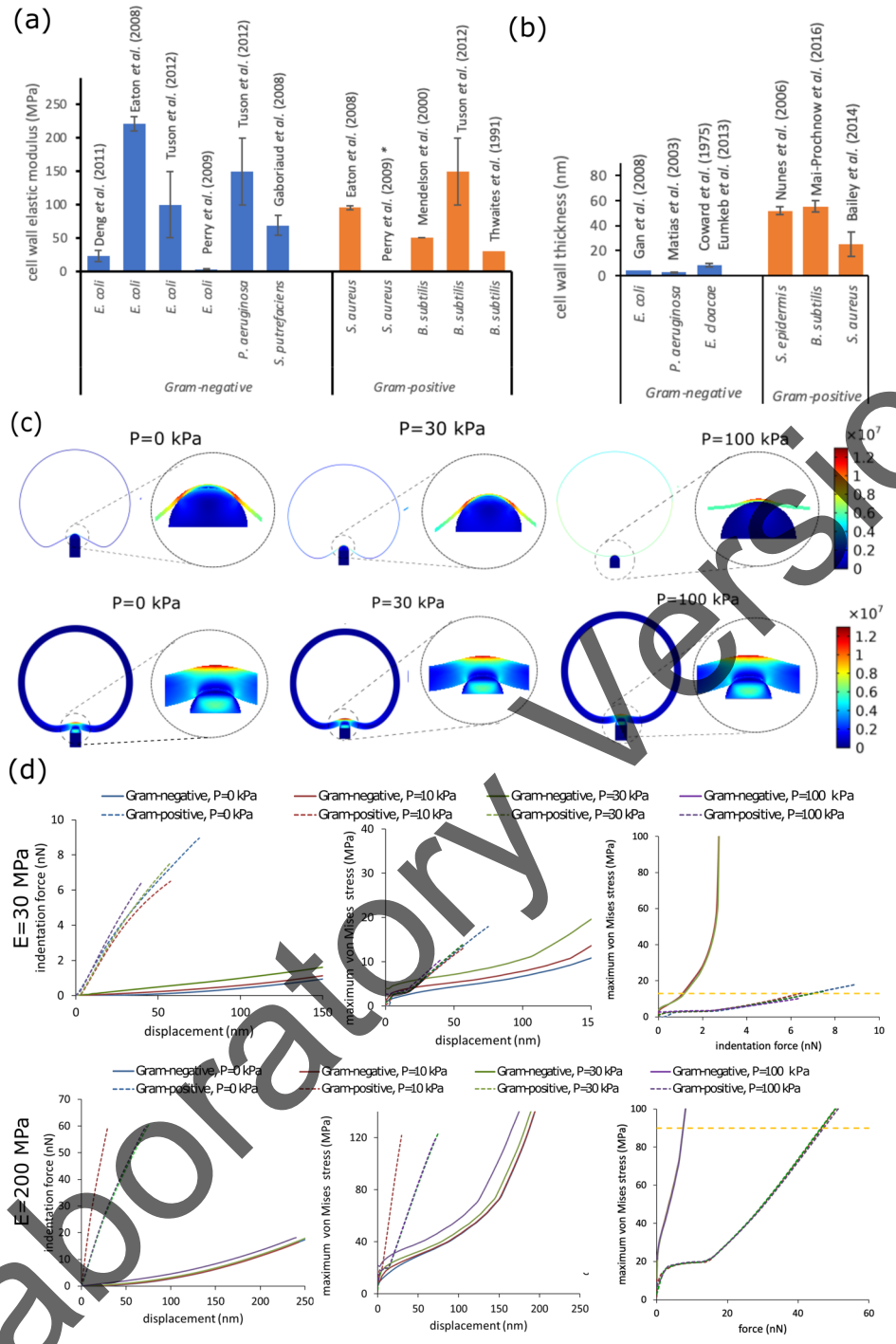

Figure 2. Effect of biomechanical parameters on the cellar deformation on nanopillars having a diameter of 50 nm. (a) Literature values of bacterial cell wall elastic modulus.[24,27,43−47] In cases in which multiple values are reported to account for anisotropy, only the smallest value is shown (in such cases, the values are still typically within the same order of magnitude). * indicates a value of 2.6 MPa. Data obtained from ref 25 Table 1 with permission, with the inclusion of additional data. (b) Literature values of bacterial cell wall thickness.[20,48−53] (c) Deformation profiles for a model Gram-positive and Gram-negative bacterium at different turgor pressure values (P) for the cell wall modulus E = 30 MPa. (d) FEA simulation outputs showing the curves for indentation force versus displacement, maximum von Mises stress versus displacement, and maximum von Mises stress versus indentation force for the cell wall modulus E = 30 MPa and 200 MPa (at P = 100 kPa and E = 30 MPa the Gram-negative bacterium's maximum von Mises stress at the floating condition, i.e., before contacting the nanopillar, is 22 MPa, exceeding the cell wall yield strength, and is therefore not shown). The yellow dashed lines show the approximated values of the cell wall tensile strength.

of biological materials have shown that such concentrated stress fields, developing upon indentation, result in cell puncture,[35] consistent with our experimental observations.[9] This view further corroborates other experimental observations. Techniques such as focused ion beam scanning electron microscopy (FIB-SEM) have provided images illustrating cell deformation and lysis resulting from the bacterial envelope being pierced by nanopillars.[36] In cases where deformation does not result in impaling, it can still significantly stretch the cell upon contact with nanopillars.[37,38] Additionally, observa-

tions indicate that cells lysed through nonpenetrating mechanisms may exhibit different interactions at the nanopillar-bacterium interface.[36] For instance, Jenkins et al. showed that entrapment of bacteria between nanopillars may give rise to cell impedance, deactivating the attached bacteria.[36]

Overall, these results show that the proposed FEA model is capable of capturing, at least qualitatively, nanopillar−bacterium interactions; it might therefore be used to conduct broader studies on various aspects of mechano-bactericidal activity.

Effect of Bacterial Mechanical Properties on Bacterial Deformation. Having analyzed the baseline model, it is pertinent to dissect deeper mechanistic aspects of mechano-bactericidal activity, namely, the effects of cell wall thickness, elastic modulus, and internal pressure. Cell wall elastic modulus is a key biomechanical property of bacteria that is largely dependent on the chemical composition and structure of the cell wall. It varies among different bacterial species depending on the characteristics of the cell wall peptidoglycan network, such as arrangement, cross-linking patterns, chain length, or degree of branching.[39] Cell wall thickness (t) is influenced by the thickness of peptidoglycan layer and varies substantially between bacterial classes, with the Gram-positive bacteria having a substantially thicker cell wall (20−80 nm) than Gram-negative bacteria (1−10 nm).[25] Turgor pressure (P) depends on the bacteria type and, in addition, is significantly affected by the cell biological state and environmental conditions, varying from hypertonic to hypotonic depending on the medium osmolarity.[40]

Despite the influence of these parameters on cell biomechanics, they have not been fully studied and decoupled with respect to mechano-bactericidal effects. Here, we address this gap by systematically examining the effects of these parameters across a relevant range of values. The cell wall elastic moduli were prescribed values of 30 and 200 MPa. This covers the range of frequently reported values for this parameter for notorious pathogens, accounting for differences in cell wall structure and measurement variations (typical variations are shown in Figure 2a). The cell wall thicknesses were set to 2.5 nm for Gram-negative *P. aeruginosa* and 25 nm for Gram-positive *S. aureus* (typical cell wall thickness values are shown in Figure 2b). The turgor pressure was considered an independent variable subject to variation upon changes in the surrounding cell environment. In our simulations, turgor pressure was assumed to be negligibly affected by air−liquid displacement as desiccation caused by air exposure occurs over long time periods.[41] Turgor pressure can span a wide range, including 0, 10, 30, and 100 kPa. In most cases, the variation of pressure before the cell touches the substrate has little impact on the bacterial shape, except for Gram-negative bacteria at low modulus (e.g., 36.1% at E = 30 MPa and 4.96% at E = 200 MPa for G^- and 2.76% at E = 30, and 0.41% at E = 200 MPa for G^+). We performed simulations independently varying each biomechanical parameter to assess its importance in nanopillar−bacteria interactions. We report our results in terms of bacterial deformation profiles in Figure 2c (E = 30 MPa) and Figure S1 (E = 200 MPa) and the force and maximum von Mises stress curves in Figure 2d.

The increase in turgor pressure in Figure 2d produces a notable increase in the stress and indentation force; however, interestingly, the maximum von Mises stress versus force curves is independent of turgor pressure. This reflects the variation of the force being offset by the change of von Mises stress. Gram-positive bacterial deformation, unlike that of Gram-negative bacteria, shows a slight sensitivity to turgor pressure, as both force and maximum von Mises stress vary only slightly with turgor pressure. This indicates the cell wall elastic rigidity is more dominant than the resistive turgor pressure effect in the mechanical behavior of Gram-positive bacteria. Qualitatively, the rigidity of Gram-positive bacteria translates into noticeable differences. Figures 2a and S1 show that the deformation of Gram-positive bacteria is accompanied by a notable stress concentration on the nanopillar apex, while that of Gram-negative bacteria is ring-shaped and concentrated in the contact zone, although it is likely that both bacteria are eventually punctured due to localized stress.

The thicker cell wall of the Gram-positive bacterium produces a shallower indentation depth, accompanied by a steep increase in the slope of the maximum von Mises stress−displacement and force−displacement curves (Figure 2d). The increase in the cell wall modulus also triggers a substantial increase in the forces and stress (Figure 2d). Unlike the turgor pressure, these competing effects in total indicate a sublinear, but still significant impact of cell rigidity (elastic modulus and cell wall thickness) on mechanical resistance. For Gram-negative bacteria, the yield force at E = 30 MPa is 1.1−1.2 nN, which is notably smaller than the 6.5−7.0 nN yield force for Gram-positive bacteria. Both values increase at E = 200 MPa, where the yield force for the former is 6−7 nN, and for the latter is 42−44 nN; these indicate that the Gram-positive bacterium consistently requires a 6-fold larger force to yield/puncture than the Gram-negative bacterium. These effects also apply to the ellipsoidal bacterial shapes used to approximate the elongated form of many bacterial species (see Figure S2).

Although experimental data on the decoupled effects of cell biomechanics is lacking, the deduced roles of cell wall mechanical properties are consistent with existing literature.[5,13,42] An ideal experimental evaluation would involve experiments on an identical bacterial strain with the ability to independently modulate target biomechanical parameters; however, this is likely impossible without the preparation of highly specialized mutants and sophisticated measurements. Instead, existing data mostly report species-to-species comparisons of the mechano-bactericidal activities. Several experimental studies have so far compared bactericidal activities against multiple species of Gram-positive and Gram-negative bacterial classes.[5,13,40] These studies assessed that Gram-positive bacteria, which have a thicker cell wall and typically larger elastic modulus, are much more resistant to the mechano-bactericidal effect than Gram-negative bacteria (e.g., in one report, 97.1% killing for Gram-negative *P. aeruginosa* versus 61.3% for Gram-positive *S. aureus*[42]). Using black silicon pillars and capillary forces as an external load, we experimentally confirmed that *S. aureus* bacteria undergo much less damage than *P. aeruginosa* under external capillary forces (Figure S3). These results, which corroborate our model predictions, indicate that the cell wall thickness and elastic modulus are likely universal determiners of the efficacy of the nanopillar bactericidal effect.

Our findings on the critical role of cell wall thickness and elastic modulus are also consistent with the hypothesized importance of cell wall biomechanical parameters in other modeling works. In Watson's study,[15] which provides a model of bacterial deformation under adhesion, cell wall thickness increases both the bending and stretching contributions and is considered inversely proportional to the tensile stress.

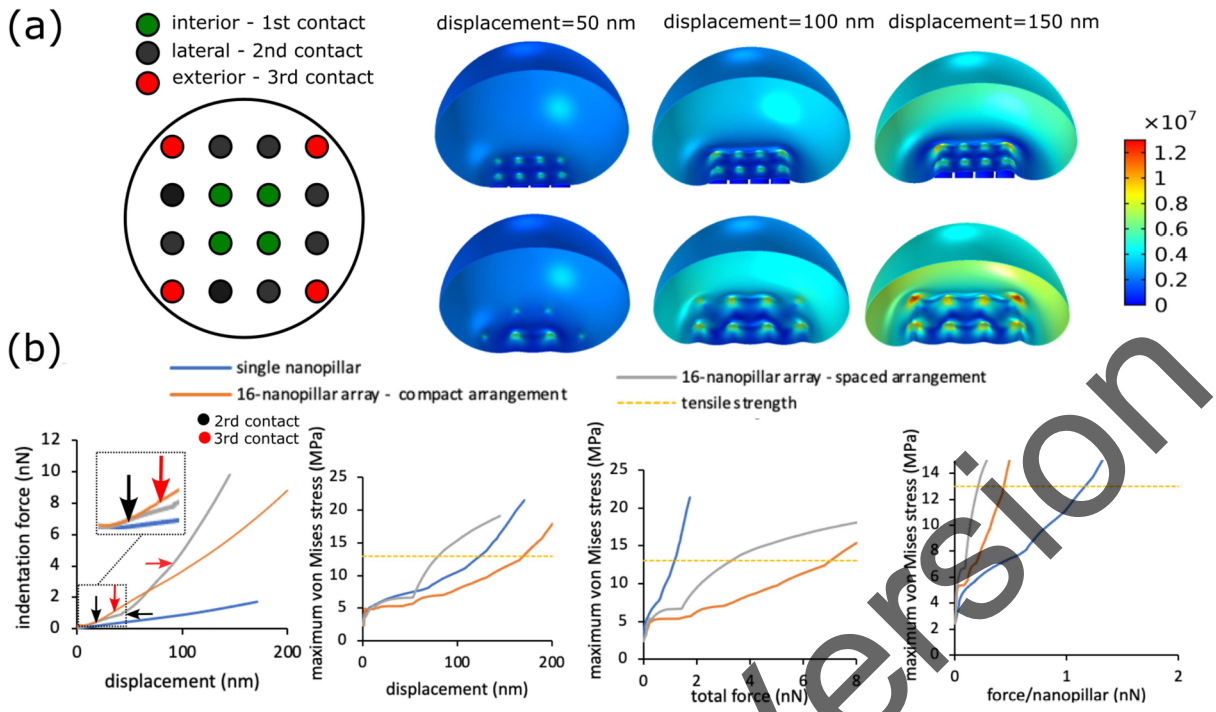

Figure 3. Bacterial deformation profile and von Mises stress upon contact with (a) a compact nanopillar array and a widely spaced array with 16 nanopillars. Only half of the geometry is shown. The left sketch shows the nanopillar labels assigned according to their position. Due to the bacterial surface curvature, nanopillars with distinct positions, i.e., interior, lateral, and exterior, contact the bacterium at different indentation depths, herein termed 1st, 2nd, and 3rd contact points. (b) Comparison of the force and stress characteristics of bacterial deformation on a single nanopillar and two arrangements of nanopillars arrays, including (from left to right) the total force (on 16 nanopillars) versus displacement, the maximum von Mises stress (over 16 nanopillars) versus displacement, the maximum von Mises versus indentation force, and the maximum von Mises versus indentation force for each nanopillar pattern. Arrows show the occurrence of contact for each distinct pillar position (see the sketch in part a); the displacement axis origin is set at the point of first contact; the vertical and horizontal arrows correspond to the compact and the widely spaced array, respectively. The yellow dashed lines show the approximated value of the cell wall tensile strength.

Comparing the cell wall tensile strength and tensile stress subsequently indicate the unlikelihood of the failure for bacteria with a larger wall thickness (e.g., >10 nm). Past FEA did not typically compare bacterial species, as each study has rather focused on a single bacterial type.[17,18,30] Nevertheless, the cell wall elasticity models and stiffness values were considered key factors in determining cell mechanical behavior.[16] Expanding on these works, our model sets forth a framework that includes the impact of turgor pressure on force and stress curves during the deformation, which further reveals the strong impacts of cell biomechanics over a wide range of conditions and mechanisms. Should more rigorous bacterial biomechanics data become available in the future, this and other models can provide a foundation for developing more rigorous numerical predictions.

Effect of Geometrical Construction. Next, given the inherent dependence of the mechano-bactericidal effect on topography, to gain better insights into mechano-bactericidal activity and criteria for designing effective antibacterial surfaces, it is of interest to analyze more complex geometries, particularly substrates with nanopillar-textured topographies. Building upon the foregoing baseline model, we compared the bacterial deformation on an array of 16 nanopillars, corresponding closely to the nanopillar densities found on artificial silicon geometries.[11] The geometry is constructed in two arrangements with differing array densities, a compact array with a center-to-center interpillar spacing of S = 60 nm and a widely spaced array with S = 100 nm. Considering the axisymmetry, the position of the nanopillars is classified as interior, exterior, and lateral (Figure 3a). Interior, lateral, and exterior nanopillars consecutively contact the bacterial surface at the "first", "second", and "third" contact points (marked in Figure 3a), causing successive interactions with 4, 12, and eventually 16 nanopillars (Figure 3b).

First, the stress diagram upon the deformation illustrates that, despite the increase in the number of nanopillars contacting the bacterium, the stress field remains focused on the contact point, again, similarly to the single-pillar scenario (Figures 3a and S4). This does not produce the strong interpillar stretch, as hypothesized in a previous work.[13] However, we see new trends in spatiotemporal contact force and stress fields. According to Figure 3a, as the bacterium is indented on the arrays and establishes contact with an increasingly larger numbers of nanopillars, the force grows at a much larger rate than that of a single nanopillar. This is plausible considering the resistance that it encounters from additional nanopillars (see the force−displacement curve in Figure 3b). However, interestingly, the value of the maximum von Mises stress, despite an initial overlap, also increases faster on arrays than on a single nanopillar (see the maximum von Mises stress−displacement curve in Figure 3b). Overall, although the increase in forces overcomes the rise in the stress to give the arrays a stronger mechanical resistance than a single nanopillar (see the force−von Mises stress curve in Figure 3b), the scaling relation of the force with the number of pillars is highly nonlinear. To reach the yield stress, the widely spaced array requires a force of 3.3 nN (at 80 nm

displacement), whereas the more compact array requires 6.9 nN (at 170 nm displacement).

To gain deeper insight into the varying forces and stresses, we further analyzed the reaction force and stress field for each type of nanopillar (Figure S5). These are highly correlated with the nanopillar positioning. The reaction force by which nanopillars counter the indentation decreases from the exterior to lateral to interior. This may be attributed to the masking effect of the surrounding nanopillars and the associated constriction in their free contact with the cell wall. On the other hand, the stress-distribution contours illustrate that the stress maxima are located on lateral and external nanopillars (after the second and third contacts, see Figure 3a). This asymmetric positioning of external nanopillars can increase the stress, rendering the cell wall more susceptible to yield. This is consistent with the higher yield force demanded by the compact array, which has a more uniform stress than that of the widely spaced array. Taken together, we infer that despite the positive contribution of each nanopillar to bacterial deformation, the extent of its influence is highly dependent on the nanopillar arrangement.

Considering the significance of these results and the lack of controlled, parametrized experimental data on the role of topographical effects in bactericidal effects caused by external forces, we assessed the validity of these predictions by conducting experiments. To this end, we fabricated silicon substrates with ordered nanopillar arrays by using e-beam lithography, a reliable technique for producing customized geometries with vertical walls. Two sets of surfaces were fabricated, one with D = 90 nm and the other with D = 200 nm, which both fall within the range of bactericidal surfaces. The former diameter corresponds to the smallest size achievable with the e-beam method for the considered aspect ratio and is reported to be highly bactericidal, while the latter serves as an example of a larger diameter, which is typically considered less bactericidal.[1,2] The tested spacings included S = 200, 300, 400, and 600 nm. The experimental assays were conducted according to our previously established protocol to produce external forces from capillary effects. Substrates were immersed in bacterial suspensions, and after bacterial attachment, the liquid was allowed to evaporate. Considering that all the patterned surfaces fall into the superhydrophilic regime, there is little variation in the magnitude of capillary forces among the surfaces (refer to SI). To preserve bacterial morphology upon exposure to these forces, bacteria were fixed immediately following evaporation (refer to Methods). Multiple methods exist to assess bactericidal effects, such as fluorescence microscopy (resolution >200−500 nm) and electron microscopy (resolution >10 nm). Fluorescence microscopy is limited in the extent to which it can resolve cell wall deformation, principally assessing membrane integrity, so SEM was adopted as the primary analytical method in this work.

Figure 4a shows morphological bacterial damage, revealing that the extent of injury varies widely. For substrates with D = 90 nm and S = 200 nm, cells (seen mostly on the top of the array) experienced minor damage, whereas increasing S to 300 and 400 nm resulted in flattening and piercing by bent nanopillars. On the surface with S = 600 nm, bacteria were completely torn apart, shrunk, and sunk into the arrays. Similar trends were observed on the surface with D = 200 nm, which is blunter, although less damage is evident as a whole. This trend is seen quantitatively in Figure 4b, where a comparison on the

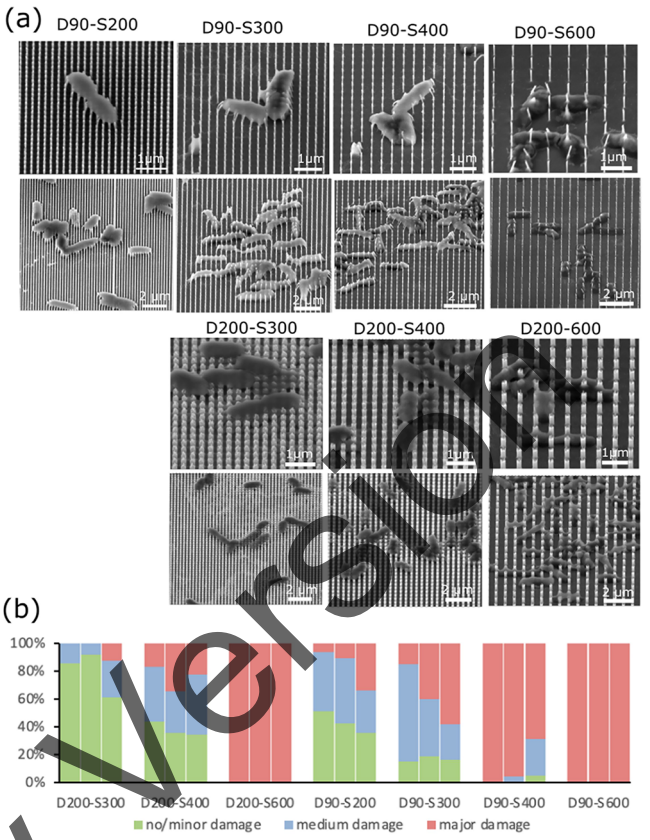

Figure 4. Experimental assessment of mechano-bactericide on ordered silicon nanopillar arrays. (a) Bacterial damage on nanopillar arrays of varying dimensions; D is the diameter and S is the center-to-center spacing. The use of e-beam lithography results in vertical walls and a smooth surface for most cases. Sometimes irregularities are seen atop the nanopillars with D = 200 nm, due to the etching effects. (b) Quantitative results of bacterial populations for three replicates for each sample (each cluster). No/minor damage: cell with minimal deformation and damage (no noticeable piercing), medium damage: notable cell deformation characterized by piercing and nanopillars bending, which was previously shown to correlate with the amount of mechano-bactericidal forces,[46] major damage: cells sunken into the bottom of the array and pierced all the way through. In some cases, the interaction between nanopillars and bacteria is so intense that it causes nanopillar bending (mainly seen for pillars with smaller diameters).

mechano-bactericidal activity was made by classifying cells into those with minor or no damage (cells remain integrated with negligible deformation), medium damage (flattened and pierced), and major damage (sunken, pierced through). This assessment of the bacterial population reveals a universal pattern across multiple samples, verifying trends set forth by the model predictions.

The observed mechanism is reminiscent of the well-known "bed of nails" effect despite the intriguing fact that the type of forces and scale of the problem are entirely different. When a person lies on a bed of nails, despite the injury that each nail may cause, the distribution of body weight among many nails reduces the load on each nail, preventing damage. To maximize the mechano-bactericidal effect, the bed-of-nails effect must be prevented. Thus, based on these results, an effective heuristic design strategy would be to increase the interpillar spacing as much as possible—potentially as long as an efficient contact between bacteria and the pillars is ensured

and below the limit in which bacteria may freely slip through without touching nanopillars. In silico models, such as those shown in Figure S6, can be used to simulate bacterial spatial distribution and the number of contact points for bacteria upon variations in interpillar spacing.

The comparison between these results and previous works shows that the effect of interpillar spacing varies with mechano-bactericidal mechanisms. In adhesion-driven mechano-bactericidal mechanisms, larger spacings were suggested to cause less damage due to the weaker binding strength between the substratum and bacteria. Cui et al., who investigated the antibacterial activity of nanopillared polycarbonate (PC) surfaces against *E. coli*, reported an interpillar spacing of 170 nm as the most bactericidal within the 100−300 nm range.[54] Wu et al. also reported a similar range for the optimal killing efficiency of OrmoStamp nanostructures against *S. aureus*.[55] On the contrary, Modaresifar et al. reported a different trend whereby decreasing the nanopillar spacing increased mechano-bactericidal activity,[56] finding 100 nm as the most efficient interspacing.[45] Results obtained from theoretical models also vary depending on the model scope and assumptions. Models simulating adhesion effects report optimal values from a balance between adhesion strength, increasing at lower spacing, and the cell wall stress effect, growing at larger spacings.[16] Mirzaali's work simulating bacterial deformation under body forces, such as bacterial weight, shows higher bacterial deformation at larger spacings.[18] Overall, despite some common features (such as the presence of an optimum value), reconciling the results across different mechanisms appears to be complex and could be additionally compounded by the coexistence of multiple mechanisms.[57] Identifying the relevant forces and estimating their magnitudes through rigorous experimental and computational approaches is an essential step in deciphering discrepancies in the literature.

Prospective Utility of the Model. Being discovered just nearly a decade ago, the mechano-bactericidal effect, which emerged as a novel paradigm to design chemical-free antibacterial materials, has been the subject of many investigations.[1,2,10] While substantial work has been carried out on demonstrating the mechano-bactericidal activity on a diverse range of materials, knowledge of the precise role of parameters is lacking and has led to contradictory results reported across different studies.[1,2,11] This is partially due to the limitations of experimental tools to resolve the bacterial physics at the nanoscale and the absence of validated experimental protocols that could be widely adopted for mechano-bactericide characterization. We attempted to systematically control experimental factors by defining sample preparation and analysis protocols that differentiate between external and internal forces. We identified influential mechanisms and parameters (such as surface hydrophobicity) that can be leveraged to enhance mechano-bactericidal activity.[9,11] Although such modifications can improve the bactericidal activity of nanopillared surfaces, several technical challenges remain; these include the need for efficient fabrication techniques across a broad range of materials and enhanced nanopillar mechanical properties. In addition, it has been shown that nonmechanical forces, such as oxidative stresses or molecular interactions with antimicrobial chemicals grafted on nanopillars, can induce bactericidal activities.[7,58] A deeper investigation of such effects and potential synergistic strategies is a valuable area to explore in future studies.

Parallel to attempts on experimental fronts, it is also important to develop computational tools to help interpret experimental hypotheses and guide future experiments. Computational modeling undertaken in this work complements analytical approaches, which are limited in their ability to assess spatiotemporal variation of forces and stress. In this work, we introduced a modeling approach that, by simple assumptions centered on biomechanical aspects of bacteria and the substrates, can fill existing gaps and provide more accurate predictions. The model, which successfully explained a variety of experimental responses to topographical and biomechanical characteristics, may be adopted to design bactericidal materials for potential use in the biomedical and environmental industries. Given the significant costs involved in the manufacturing and testing of design prototypes, topographical parameters on substrate designs may be optimized by leveraging the proposed computational approach. While the model was adapted to a limited number of scenarios in this study, it may be customized for each use case involving a specific nanopillar geometry, bacterial size, and properties. One obstacle in mechano-bactericidal modeling is the lack of a comprehensive database of cellular properties. This partly arises from the difficulty in measuring properties at small scales and the lack of robust computational toolboxes to analyze the instrumental outputs. While improving experimental protocols can guarantee better results, using more effective computational models, such as the one here, may improve the analysis of assays such as atomic force microscopy cellular indentations.

CONCLUSIONS

In this study, FEA provided new insights into bacterial deformation on nanopillars. Nanopillar bactericidal property originates from its geometrical ability to intensify the stress on the contact area, which could induce cell wall puncture. We confirmed that the mechanical yield of bacteria by nanopillars could result from any external force of sufficiently high magnitude, demonstrating the significant role of cell physical properties in bactericidal efficacy. Cell wall rigidity, as determined by its elastic modulus and thickness, substantially affected the bacterial susceptibility to external forces. Turgor pressure substantially impacted the magnitude of contact force and cell wall stress; however, the offset effect of these two revealed a negligible contribution to the cell rupture susceptibility. Finally, nanopillar arrays were demonstrated to have different force and stress characteristics in comparison to a single nanopillar. Most importantly, we experimentally and computationally unveiled that denser nanopillar arrays have weaker bactericidal effects, pointing toward the well-known bed-of-nails effect. The ability of FEA to elucidate the mechano-bactericidal mechanism and its key determinants can promote its use in future research on mechano-bactericidal materials.

Supporting Information

The Supporting Information is available free of charge at https://pubs.acs.org/doi/10.1021/acsami.3c09552.

Summary of previous computational studies on bacter-icidal deformations, simulation results for bacteria with higher elastic modulus, simulation results for ellipsoidal bacteria, experimental data on bacterial deformation in a 3D model, description of surface wettability conditions, and stochastic simulation of bacterial distribution on nanopillar arrays.

ACKNOWLEDGMENTS

This research was supported, in part, by the Natural Sciences and Engineering Research Council of Canada (NSERC) and the McGill Interdisciplinary Initiative in Infection and Immunity (MI4) funding (NT). We acknowledge the support of the Canada Foundation for Innovation, the Canada Research Chairs program (NT, CM), the McGill Engineering Doctoral Award (AV), and the EUL fund at McGill (AV). LN2 is an International Research Laboratory (IRL) funded and co-operated by Université de Sherbrooke (UdeS), Centre National de la Recherche Scientifique (CNRS), École Centrale Lyon (ECL), Institut National des Sciences Appliquées de Lyon (INSA Lyon), and Université Grenoble Alpes (UGA). It is also financially s upported b y t he F onds d e R echerche du Québec Nature et Technologies (FRQNT). We are also grateful to the Facility for Electron Microscopy Research at McGill University and CMC Microsystems for access to simulation software. RJH acknowledges the support of an NSERC Discovery grant.

REFERENCES

(1) Tripathy, A.; Sen, P.; Su, B.; Briscoe, W. H. Natural and Bioinspired Nanostructured Bactericidal Surfaces. *Adv. Colloid Interface Sci.* **2017**, *248*, 85−104.

(2) Lin, N.; Berton, P.; Moraes, C.; Rogers, R. D.; Tufenkji, N. Nanodarts, Nanoblades, and Nanospikes: Mechano-Bactericidal Nanostructures and Where to Find Them. *Advances in colloid and interface science* **2018**, *252*, 55−68.

(3) Zhou, C.; Koshani, R.; O'Brien, B.; Ronholm, J.; Cao, X.; Wang, Y. Bio-Inspired Mechano-Bactericidal Nanostructures: A Promising Strategy for Eliminating Surface Foodborne Bacteria. *Current Opinion in Food Science* **2021**, *39*, 110−119.

(4) Bandara, C. D.; Singh, S.; Afara, I. O.; Wolff, A.; Tesfamichael, T.; Ostrikov, K.; Oloyede, A. Bactericidal Effects of Natural Nanotopography of Dragonfly Wing on Escherichia Coli. *ACS Appl. Mater. Interfaces* **2017**, *9*, 6746−6760.

(5) Doll, P. W.; Doll, K.; Winkel, A.; Thelen, R.; Ahrens, R.; Stiesch, M.; Guber, A. E. Influence of the Available Surface Area and Cell Elasticity on Bacterial Adhesion Forces on Highly Ordered Silicon Nanopillars. *ACS Omega* **2022**, *7*, 17620−17631.

(6) Linklater, D. P.; Baulin, V. A.; Juodkazis, S.; Crawford, R. J.; Stoodley, P.; Ivanova, E. P. Mechano-Bactericidal Actions of Nanostructured Surfaces. *Nature Reviews Microbiology* **2021**, *19*, 8−22.

(7) Jenkins, J.; Mantell, J.; Neal, C.; Gholinia, A.; Verkade, P.; Nobbs, A. H.; Su, B. Antibacterial Effects of Nanopillar Surfaces Are Mediated by Cell Impedance, Penetration and Induction of Oxidative Stress. *Nat. Commun.* **2020**, *11*, 1626.

(8) Hasan, J.; Crawford, R. J.; Ivanova, E. P. Antibacterial Surfaces: The Quest for a New Generation of Biomaterials. *Trends Biotechnol* **2013**, *31*, 295−304.

(9) Valiei, A.; Lin, N.; Bryche, J.-F.; McKay, G.; Canva, M.; Charette, P. G.; Nguyen, D.; Moraes, C.; Tufenkji, N. Hydrophilic Mechano-Bactericidal Nanopillars Require External Forces to Rapidly Kill Bacteria. *Nano Lett.* **2020**, *20*, 5720−5727.

(10) Ivanova, E. P.; Hasan, J.; Webb, H. K.; Truong, V. K.; Watson, G. S.; Watson, J. A.; Baulin, V. A.; Pogodin, S.; Wang, J. Y.; Tobin, M. J.; Löbbe, C.; Crawford, R. J. Natural Bactericidal Surfaces: Mechanical Rupture of Pseudomonas Aeruginosa Cells by Cicada Wings. *Small* **2012**, *8*, 2489−2494.

(11) Valiei, A.; Lin, N.; McKay, G.; Nguyen, D.; Moraes, C.; Hill, R. J.; Tufenkji, N. Surface Wettability Is a Key Feature in the Mechano-Bactericidal Activity of Nanopillars. *ACS Appl. Mater. Interfaces* **2022**, *14*, 27564−27574.

(12) Xue, F.; Liu, J.; Guo, L.; Zhang, L.; Li, Q. Theoretical Study on the Bactericidal Nature of Nanopatterned Surfaces. *J. Theor. Biol.* **2015**, *385*, 1−7.

(13) Pogodin, S.; Hasan, J.; Baulin, V. A.; Webb, H. K.; Truong, V. K.; Phong Nguyen, T. H.; Boshkovikj, V.; Fluke, C. J.; Watson, G. S.; Watson, J. A.; Crawford, R. J.; Ivanova, E. P. Biophysical Model of Bacterial Cell Interactions with Nanopatterned Cicada Wing Surfaces. *Biophys. J.* **2013**, *104*, 835−840.

(14) Li, X. Bactericidal Mechanism of Nanopatterned Surfaces. *Phys. Chem. Chem. Phys.* **2016**, *18*, 1311−1316.

(15) Watson, G. S.; Green, D. W.; Watson, J. A.; Zhou, Z.; Li, X.; Cheung, G. S. P.; Gellender, M. A Simple Model for Binding and Rupture of Bacterial Cells on Nanopillar Surfaces. *Advanced Materials Interfaces* **2019**, *6*, No. 1801646.

(16) Velic, A.; Hasan, J.; Li, Z.; Yarlagadda, P. Mechanics of Bacterial Interaction and Death on Nanopatterned Surfaces. *Biophys. J.* **2021**, *120*, 217−231.
(17) Cui, Q.; Liu, T.; Li, X.; Zhao, L.; Wu, Q.; Wang, X.; Song, K.; Ge, D. Validation of the Mechano-Bactericidal Mechanism of Nanostructured Surfaces with Finite Element Simulation. *Colloids Surf., B* **2021**, *206*, No. 111929.
(18) Mirzaali, M. J.; van Dongen, I. C. P.; Tümer, N.; Weinans, H.; Yavari, S. A.; Zadpoor, A. A. In-Silico Quest for Bactericidal but Non-Cytotoxic Nanopatterns. *Nanotechnology* **2018**, *29*, 43LT02.
(19) Islam, M.; Aldawsari, F. S. S.; Yarlagadda, P. K. D. V. Finite Element Modelling of a Gram-Negative Bacterial Cell and Nanospike Array for Cell Rupture Mechanism Study. *Molecules* **2023**, *28* (5), 2184.
(20) Mai-Prochnow, A.; Clauson, M.; Hong, J.; Murphy, A. B. Gram Positive and Gram Negative Bacteria Differ in Their Sensitivity to Cold Plasma. *Sci. Rep.* **2016**, *6*, 38610.
(21) Giesbrecht, P.; Kersten, T.; Maidhof, H.; Wecke, J. Staphylococcal Cell Wall: Morphogenesis and Fatal Variations in the Presence of Penicillin. *Microbiology and molecular biology reviews: MMBR* **1998**, *62*, 1371−1414.
(22) Silhavy, T. J.; Kahne, D.; Walker, S. The Bacterial Cell Envelope. *Cold Spring Harbor perspectives in biology* **2010**, *2*, a000414−a000414.
(23) Huang, K. C.; Mukhopadhyay, R.; Wen, B.; Gitai, Z.; Wingreen, N. S. Cell Shape and Cell-Wall Organization in Gram-Negative Bacteria. *Proc. Natl. Acad. Sci. U. S. A.* **2008**, *105*, 19282−19287.
(24) Thwaites, J. J.; Surana, U. C. Mechanical Properties of Bacillus Subtilis Cell Walls: Effects of Removing Residual Culture Medium. *J. Bacteriol.* **1991**, *173*, 197−203.
(25) Elbourne, A.; Chapman, J.; Gelmi, A.; Cozzolino, D.; Crawford, R. J.; Truong, V. K. Bacterial-Nanostructure Interactions: The Role of Cell Elasticity and Adhesion Forces. *J. Colloid Interface Sci.* **2019**, *546*, 192−210.
(26) Jiang, H.; Si, F.; Margolin, W.; Sun, S. X. Mechanical Control of Bacterial Cell Shape. *Biophys. J.* **2011**, *101* (2), 327−335.
(27) Deng, Y.; Sun, M.; Shaevitz, J. W. Direct Measurement of Cell Wall Stress Stiffening and Turgor Pressure in Live Bacterial Cells. *Phys. Rev. Lett.* **2011**, *107*, No. 158101.
(28) Hopcroft, M. A.; Nix, W. D.; Kenny, T. W. What Is the Young's Modulus of Silicon? *Journal of microelectromechanical systems* **2010**, *19*, 229−238.
(29) Valiei, A.; Okshevsky, M.; Lin, N.; Tufenkji, N. Anodized Aluminum with Nanoholes Impregnated with Quaternary Ammonium Compounds Can Kill Pathogenic Bacteria within Seconds of Contact. *ACS Appl. Mater. Interfaces* **2018**, *10*, 41207−41214.
(30) Velic, A.; Jaggessar, A.; Tesfamichael, T.; Li, Z.; Yarlagadda, P. K. D. V. Effects of Nanopillar Size and Spacing on Mechanical Perturbation and Bactericidal Killing Efficiency. *Nanomaterials* **2021**, *11*, 2472.
(31) Volokh, K. Y. Modeling Failure of Soft Anisotropic Materials with Application to Arteries. *J. Mech Behav Biomed Mater.* **2011**, *4*, 1582−1594.
(32) Suo, Z.; Avci, R.; Deliorman, M.; Yang, X.; Pascual, D. W. Bacteria Survive Multiple Puncturings of Their Cell Walls. *Langmuir* **2009**, *25*, 4588−4594.
(33) Liu, S.; Ng, A. K.; Xu, R.; Wei, J.; Tan, C. M.; Yang, Y.; Chen, Y. Antibacterial Action of Dispersed Single-Walled Carbon Nanotubes on Escherichia Coli and Bacillus Subtilis Investigated by Atomic Force Microscopy. *Nanoscale* **2010**, *2*, 2744−2750.
(34) Del Valle, A.; Torra, J.; Bondia, P.; Tone, C. M.; Pedraz, P.; Vadillo-Rodriguez, V.; Flors, C. Mechanically Induced Bacterial Death Imaged in Real Time: A Simultaneous Nanoindentation and Fluorescence Microscopy Study. *ACS Appl. Mater. Interfaces* **2020**, *12*, 31235−31241.
(35) Liu, J.; Chen, Z.; Liang, X.; Huang, X.; Mao, G.; Hong, W.; Yu, H.; Qu, S. Puncture Mechanics of Soft Elastomeric Membrane with Large Deformation by Rigid Cylindrical Indenter. *Journal of the Mechanics and Physics of Solids* **2018**, *112*, 458−471.
(36) Jenkins, J.; Ishak, M. I.; Eales, M.; Gholinia, A.; Kulkarni, S.; Keller, T. F.; May, P. W.; Nobbs, A. H.; Su, B. Resolving Physical Interactions between Bacteria and Nanotopographies with Focused Ion Beam Scanning Electron Microscopy. *iScience* **2021**, *24*, No. 102818.
(37) Bandara, C. D.; Ballerin, G.; Leppänen, M.; Tesfamichael, T.; Ostrikov, K. K.; Whitchurch, C. B. Resolving Bio−Nano Interactions of E. Coli Bacteria−Dragonfly Wing Interface with Helium Ion and 3D-Structured Illumination Microscopy to Understand Bacterial Death on Nanotopography. *ACS Biomaterials Science & Engineering* **2020**, *6*, 3925−3932.
(38) Ishak, M. I.; Jenkins, J.; Kulkarni, S.; Keller, T. F.; Briscoe, W. H.; Nobbs, A. H.; Su, B. Insights into Complex Nanopillar-Bacteria Interactions: Roles of Nanotopography and Bacterial Surface Proteins. *J. Colloid Interface Sci.* **2021**, *604*, 91−103.
(39) Auer, G. K.; Weibel, D. B. Bacterial Cell Mechanics. *Biochemistry* **2017**, *56*, 3710−3724.
(40) Rojas, E. R.; Huang, K. C. Regulation of Microbial Growth by Turgor Pressure. *Curr. Opin. Microbiol.* **2018**, *42*, 62−70.
(41) Potts, M. Desiccation Tolerance of Prokaryotes. *Microbiol. Rev.* **1994**, *58* (4), 755−805.
(42) Truong, V. K.; Geeganagamage, N. M.; Baulin, V. A.; Vongsvivut, J.; Tobin, M. J.; Luque, P.; Crawford, R. J.; Ivanova, E. P. The Susceptibility of Staphylococcus Aureus CIP 65.8 and Pseudomonas Aeruginosa ATCC 9721 Cells to the Bactericidal Action of Nanostructured Calopteryx Haemorrhoidalis Damselfly Wing Surfaces. *Appl. Microbiol. Biotechnol.* **2017**, *101*, 4683−4690.
(43) Eaton, P.; Fernandes, J. C.; Pereira, E.; Pintado, M. E.; Xavier Malcata, F. Atomic Force Microscopy Study of the Antibacterial Effects of Chitosans on Escherichia Coli and Staphylococcus Aureus. *Ultramicroscopy* **2008**, *108*, 1128−1134.
(44) Mendelson, N. H.; Sarlls, J. E.; Wolgemuth, C. W.; Goldstein, R. E. Chiral Self-Propulsion of Growing Bacterial Macrofibers on a Solid Surface. *Phys. Rev. Lett.* **2000**, *84*, 1627−1630.
(45) Perry, C. C.; Weatherly, M.; Beale, T.; Randriamahefa, A. Atomic Force Microscopy Study of the Antimicrobial Activity of Aqueous Garlic versus Ampicillin against Escherichia Coli and Staphylococcus Aureus. *Journal of the Science of Food and Agriculture* **2009**, *89*, 958−964.
(46) Tuson, H. H.; Auer, G. K.; Renner, L. D.; Hasebe, M.; Tropini, C.; Salick, M.; Crone, W. C.; Gopinathan, A.; Huang, K. C.; Weibel, D. B. Measuring the Stiffness of Bacterial Cells from Growth Rates in Hydrogels of Tunable Elasticity. *Mol. Microbiol.* **2012**, *84*, 874−891.
(47) Gaboriaud, F.; Parcha, B. S.; Gee, M. L.; Holden, J. A.; Strugnell, R. A. Spatially Resolved Force Spectroscopy of Bacterial Surfaces Using Force-Volume Imaging. *Colloids Surf., B* **2008**, *62*, 206−213.
(48) Gan, L.; Chen, S.; Jensen, G. J. Molecular Organization of Gram-Negative Peptidoglycan. *Proc. Natl. Acad. Sci. U. S. A.* **2008**, *105*, 18953−18957.
(49) Matias, V. R.; Al-Amoudi, A.; Dubochet, J.; Beveridge, T. J. Cryo-Transmission Electron Microscopy of Frozen-Hydrated Sections of Escherichia Coli and Pseudomonas Aeruginosa. *J. Bacteriol.* **2003**, *185*, 6112−6118.
(50) Coward, J. E.; Rosenkranz, H. S. Electron Microscopic Appearance of Silver Sulfadiazine-Treated Enterobacter Cloacae. *Chemotherapy* **2004**, *21*, 231−235.
(51) Eumkeb, G.; Chukrathok, S. Synergistic Activity and Mechanism of Action of Ceftazidime and Apigenin Combination against Ceftazidime-Resistant Enterobacter Cloacae. *Phytomedicine* **2013**, *20*, 262−269.
(52) Nunes, A. P. F.; Teixeira, L. M.; Iorio, N. L. P.; Bastos, C. C. R.; Fonseca, L. de S.; Souto-Padrón, T.; dos Santos, K. R. N. Heterogeneous Resistance to Vancomycin in Staphylococcus Epidermidis, Staphylococcus Haemolyticus and Staphylococcus Warneri Clinical Strains: Characterisation of Glycopeptide Susceptibility Profiles and Cell Wall Thickening. *Int. J. Antimicrob. Agents* **2006**, *27*, 307−315.

(53) Bailey, R. G.; Turner, R. D.; Mullin, N.; Clarke, N.; Foster, S. J.; Hobbs, J. K. The Interplay between Cell Wall Mechanical Properties and the Cell Cycle in Staphylococcus Aureus. *Biophys. J.* **2014**, *107*, 2538−2545.
(54) Cui, Q.; Liu, T.; Li, X.; Song, K.; Ge, D. Nanopillared Polycarbonate Surfaces Having Variable Feature Parameters as Bactericidal Coatings. *ACS Applied Nano Materials* **2020**, *3*, 4599−4609.
(55) Wu, S.; Zuber, F.; Maniura-Weber, K.; Brugger, J.; Ren, Q. Nanostructured Surface Topographies Have an Effect on Bactericidal Activity. *J. Nanobiotechnol.* **2018**, *16*, 20.
(56) Modaresifar, K.; Kunkels, L. B.; Ganjian, M.; Tümer, N.; Hagen, C. W.; Otten, L. G.; Hagedoorn, P. L.; Angeloni, L.; Ghatkesar, M. K.; Fratila-Apachitei, L. E.; Zadpoor, A. A. Deciphering the Roles of Interspace and Controlled Disorder in the Bactericidal Properties of Nanopatterns against Staphylococcus Aureus. *Nanomaterials (Basel)* **2020**, *10*, 347.
(57) Ivanova, E. P.; Linklater, D. P.; Werner, M.; Baulin, V. A.; Xu, X.; Vrancken, N.; Rubanov, S.; Hanssen, E.; Wandiyanto, J.; Truong, V. K.; Elbourne, A.; Maclaughlin, S.; Juodkazis, S.; Crawford, R. J. The Multi-Faceted Mechano-Bactericidal Mechanism of Nanostructured Surfaces. *Proc. Natl. Acad. Sci. U. S. A.* **2020**, *117*, 12598−12605.
(58) Wang, H.; Wang, L.; Zhang, P.; Yuan, L.; Yu, Q.; Chen, H. High Antibacterial Efficiency of pDMAEMA Modified Silicon Nanowire Arrays. *Colloids Surf., B* **2011**, *83*, 355−359.

Supporting Information

Effects of surface topography and cellular biomechanics on nanopillar-induced bactericidal activity

DOI: https://doi.org/10.1021/acsami.3c09552

Amin Valiei[1*], Jean-François Bryche[2,3], Michael Canva[2,3], Paul G. Charette[2,3], Christopher Moraes[1,4,5], Reghan J. Hill[1*], and Nathalie Tufenkji[1]

[1]Department of Chemical Engineering, McGill University, Montreal, Québec H3A 0C5, Canada.

[2]Laboratoire Nanotechnologies Nanosystèmes (LN2)-IRL3463, CNRS, Université de Sherbrooke, Université Grenoble Alpes, École Centrale de Lyon, INSA Lyon, Sherbrooke, Québec J1K 0A5, Canada

[3]Institut Interdisciplinaire d'Innovation Technologique (3IT), Université de Sherbrooke, 3000 Boulevard de l'Université, Sherbrooke, Québec J1K OA5, Canada.

[4]Department of Biomedical Engineering, McGill University, Montreal, Québec H3A 0C5, Canada

[5]Goodman Cancer Research Center, McGill University, Montreal, Québec H3A 0G4, Canada.

*Corresponding authors: amin.valiei@mail.mcgill.ca, reghan.hill@mcgill.ca

Table S1. Previous finite element modeling studies on bactericidal deformations on nanopillars

Article	Cell wall model	Cytoplasm model	Bactericidal force	Surface material	Bacterial features	Force value	Dimensions	Findings
Mirzaali *et al.*[1]	linear elastic	visco-hyperelastic material	gravity, buoyancy	silicon	*S. aureus*	5.57×10^{-2} N/mm^2 Water column 0.794 N/mm^2	W: 25-200 nm, IS (interspacing): 40-300 nm	nanopillars with shorter widths and interspacing substantially increase bactericidal effects
Cui *et al.*[2]	elastic, linear viscoelastic, plastic creep	constant turgor pressure	adhesion	silicon - titanium	*E. coli*	5 nN (6.5 kPa)	D: 20− 200 nm, S (center-to-center spacing): 100− 300 nm, H = 200 nm	too large or too small nanopillar spacing reduces stress exerted on cells by nanopillars
Velic *et al.*[3]	orthotropic elastic (isotropic neo Hookean)	NA	adhesion	rigid material	Gram-negative	1–40 mJ/m^2	D: 60 nm (variation: 20-180 nm), S (center-to-center spacing): 180 (S/D variation: 2-4), H= 200 nm (variation: 100-300 nm)	no variation in maximal envelope strain when changing interspacing (up to 10 mJ/m^2 adhesion energy)
Islam *et al.*[4]	elastic	constant turgor pressure	contact with increasing turgor pressure	rigid material	*E. coli*	maximum strain energy: 0.8 J	D: 30 nm. S (center-to-center spacing: 200 nm)	bacteria-nanopillar interaction punctures cell wall

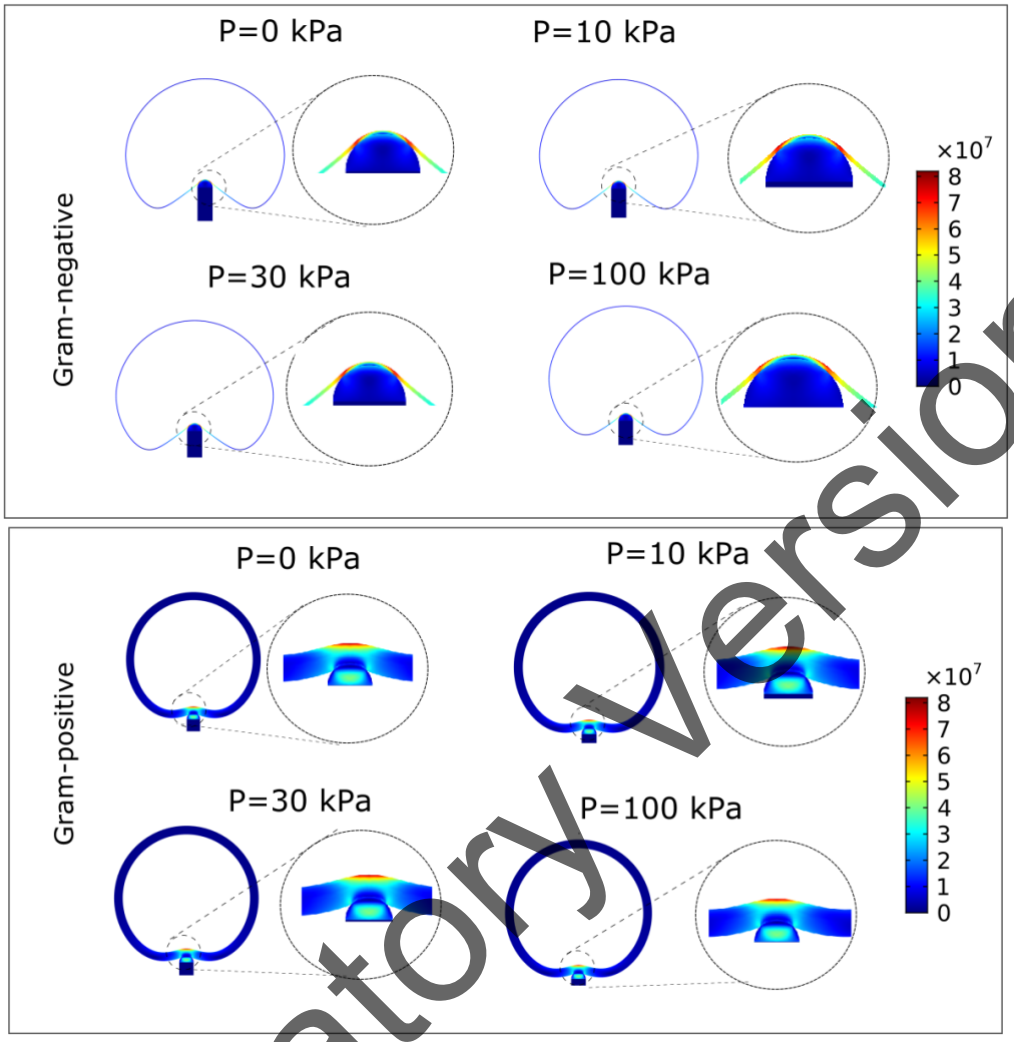

Figure S1. Bacterial deformation profiles for a model Gram-positive and a Gram-negative bacterium at different values of the turgor pressure (P) and elastic modulus E=200 MPa.

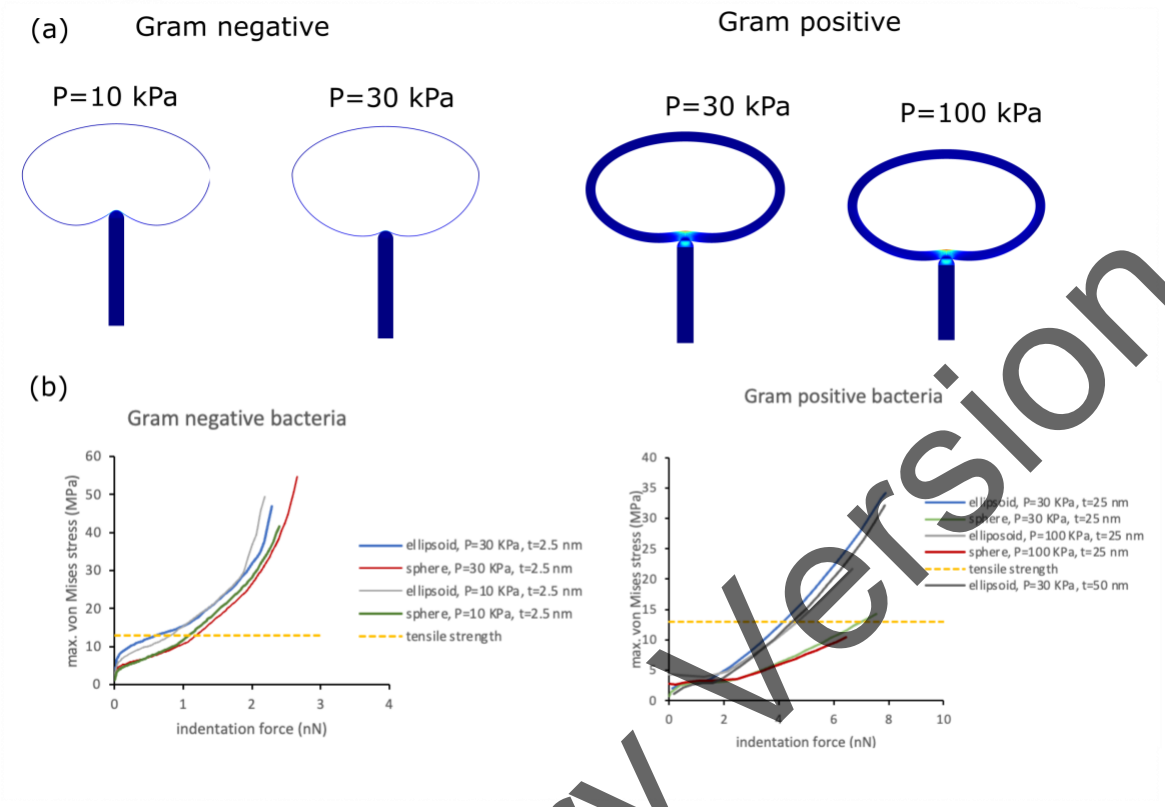

Figure S2. Deformation profiles for ellipsoidal bacteria (length=1500 mm, width=500 mm) including model Gram-positive and Gram-negative types (b) force *versus* maximum von Mises stress for various bacterial shapes and internal pressures.

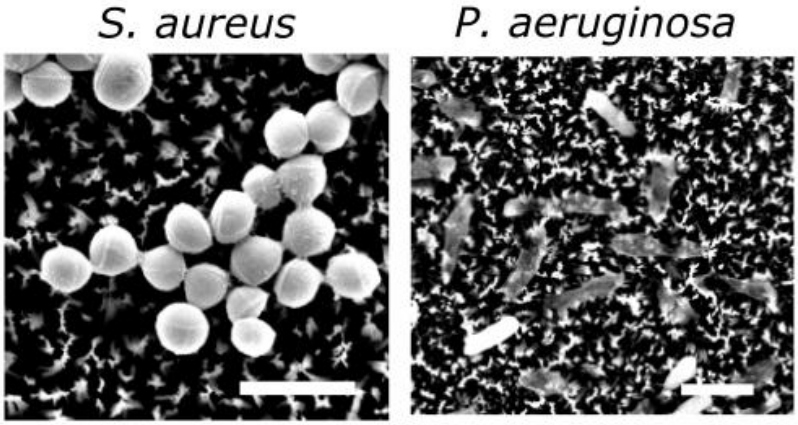

Figure S3. Comparison of response between the Gram-positive (*S. aureus*) and Gram-negative (*P. aeruginosa*) upon contact with chemically etched silicon nanopillars, characterized in our previous studies [5,6]. Both bacteria were exposed to capillary forces developing during water/air displacement, using a protocol similar to our previous work [5]. While the Gram-positive bacteria remain morphologically intact, Gram-negative counterparts undergo significant structural damage. Scale bar=2 μm (SEM Acceleration voltage=5 kV).

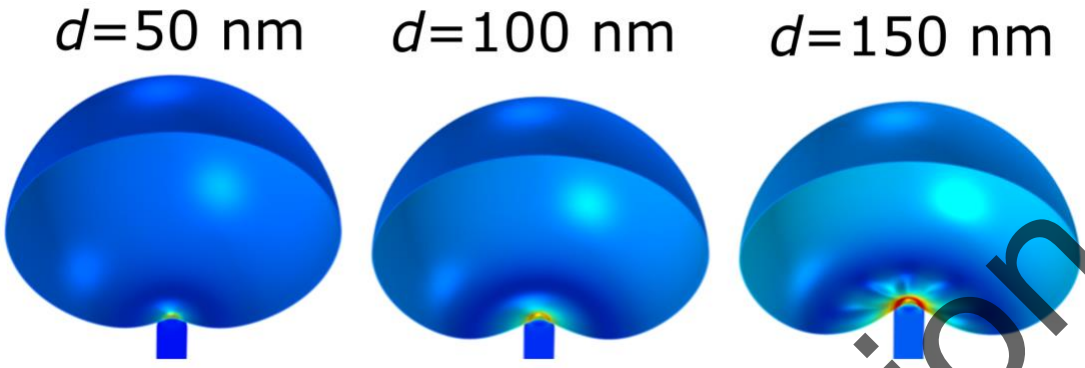

Figure S4. Bacterial deformation against a single nanopillar in the 3D model.

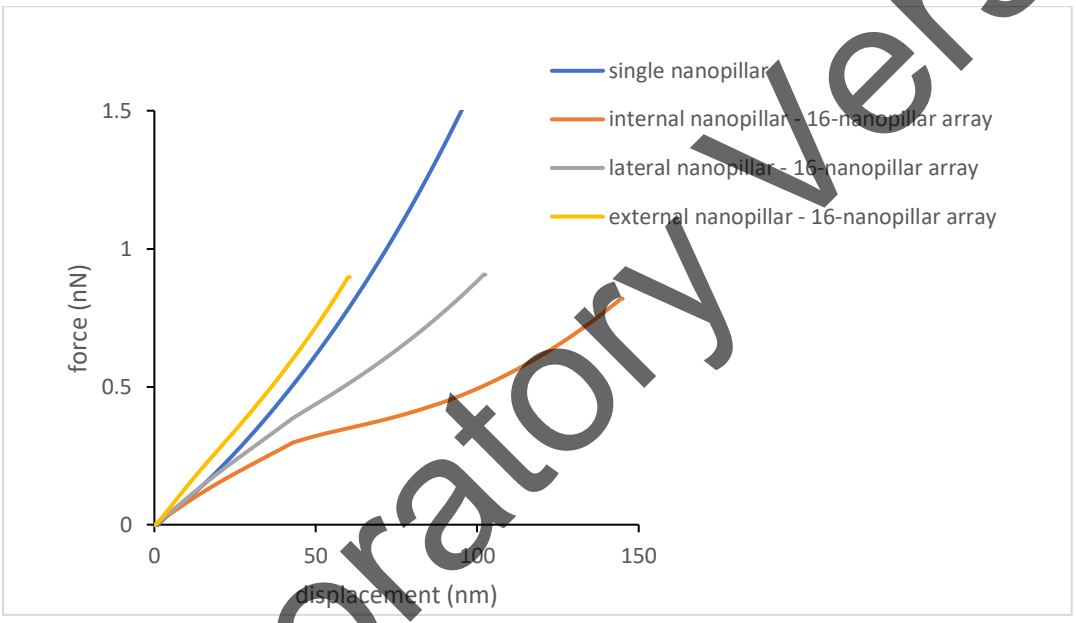

Figure S5. Nanopillar reaction forces for a nanopillar array comprising 16 nanopillars with diameter 50 nm and interpillar spacing 100 nm. Nanopillars are classified as interior, lateral, and exterior (see Figure 3a).

Wetting conditions for different interpillar spacings

The area having a nanopillar pattern in this work is fabricated using e-beam lithography, a method known for its high precision but low throughput. Accordingly, the patterned segment is relatively small (200 μm×200 μm). For this reason, it was not feasible to measure the droplet contact angle using a contact angle goniometer. However, the contact angle can be estimated using the Wenzel equation [7].

According to the Wenzel equation, the apparent contact angle on a topographic surface is related to the intrinsic contact angle on a flat surface of the same material through the roughness factor. The roughness factor represents the ratio of the geometric surface area to the projected (flat) surface area. For hydrophilic surfaces, the presence of roughness tends to make the surface even more hydrophilic. When the roughness factor falls below a certain threshold, the surface becomes completely wet.

In the table below, we have calculated the roughness factor for various pillar spacings and, consequently, determined the intrinsic contact angle cutoff that ensures complete surface wetting (apparent contact angle approaching zero). Notably, in all cases, the cut-off value is below our flat surface contact angle of 29°, indicating that the patterned area becomes completely wet. Based on these results, the interspacing variation has little impact on the value of the capillary forces, suggesting that these forces can be assumed to be identical on all tested substrates—the correlation between capillary forces and surface hydrophobicity is discussed in our previous studies [5,6].

Roughness ratio (patterned area/flat area)	Intrinsic contact angle (flat)
4.53	77°
1.88	58°
1.39	44°

Simulation of bacterial distribution on nanopillar arrays

Figure S6 summarizes the analysis of simulations of bacterial populations randomly placed on nanopillar arrays with varying nanopillar spacing *S*.

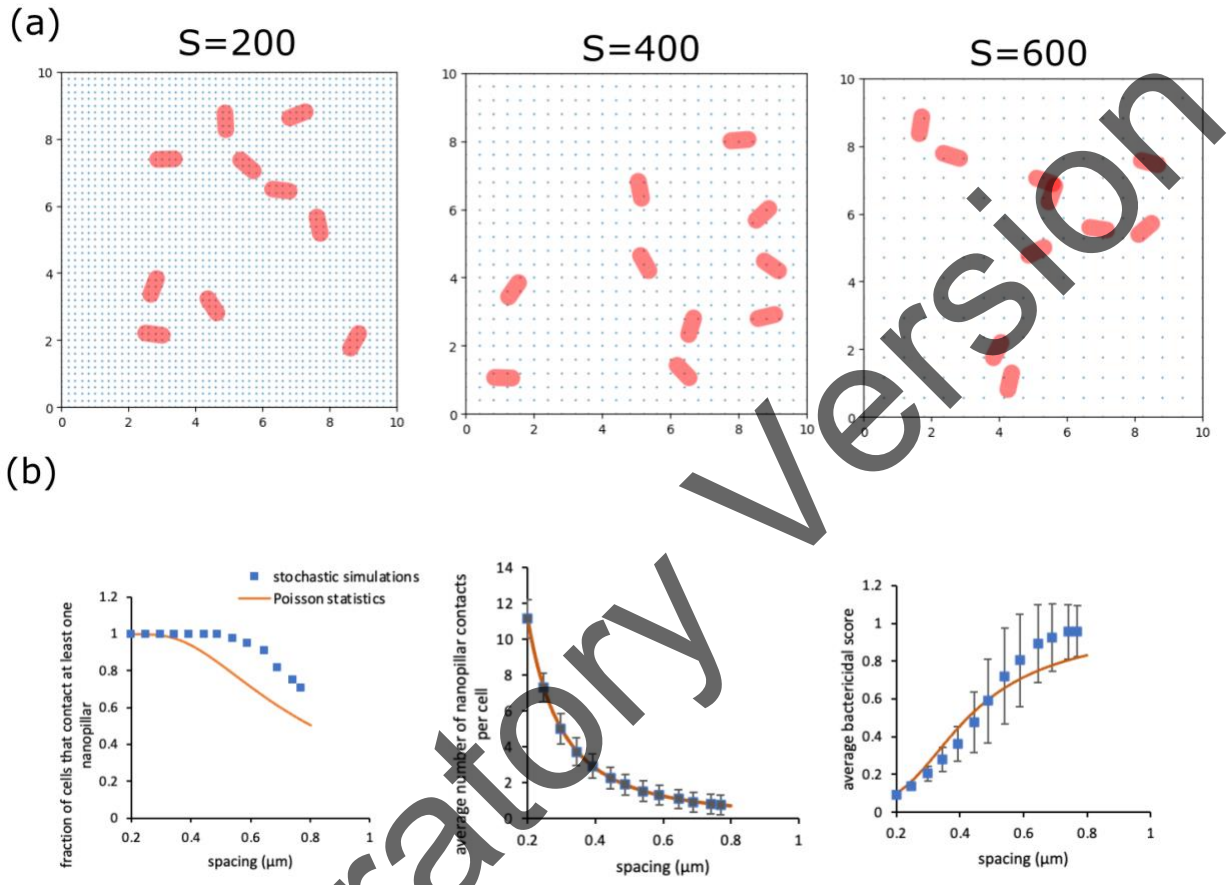

Figure S6. Stochastic simulations and their Poisson-statistics approximation of bacterial cells randomly placed on square nanopillar arrays (varying interpillar spacing *S*). (a) Illustrations of bacterial cells randomly placed on nanopillar arrays with dense to sparse nanopillar spacings. Analysis shows that, for S<0.6 μm, more than 95% of bacteria contact at least one nanopillar (bacterial area=0.45 μm^2, length=1.5 μm, width=0.5 μm; nanopillar diameter=50 nm). (b) Analysis of simulations undertaken with 500 cells on each array (circles): (left) Fraction of cells contacting at least one nanopillar decreases with increasing nanopillar spacing, qualitatively as predicted by Poisson statistics (random nanopillar positions with the same nanopillar number density, solid lines); (middle) average number of nanopillar contacts per cell decreases as predicted by Poisson statistics (A/S^2); (right) the number of nanopillar contacts per cell can be used to calculate a bactericidal efficiency for each cell. For demonstrative purposes, the graph shows the bactericidal efficiency, approximated as the average reciprocal number of contacts per cell, for the population of cells that contact at least one nanopillar. Error bars are the standard deviation.

According to Poisson statistics, the probability of x nanopillar contacts per cell is

$$P(x) = \frac{e^{-\lambda}\lambda^x}{x!},$$

where

$$\lambda = \frac{A}{S^2}$$

is the average number of nanopillar contacts per cell, *A* is the cell area, and *S* is the center-to-center nanopillar spacing ($1/S^2$ is the nanopillar areal number density). The fraction of cells contacting at least one nanopillar is

$$1 - P(0) = 1 - e^{-\lambda},$$

and the average bactericidal score is

$$G(\lambda) = \frac{\sum_{x=1}^{x=\lfloor A/D^2 \rfloor} P(x)\frac{1}{x}}{\sum_{x=1}^{x=\lfloor A/D^2 \rfloor} P(x)},$$

where *D* is the nanopillar diameter. The upper limit of the sums, $A/D^2=180$, is the maximum number of nanopillar contacts (this may be extended to infinity for $S>>D$).

Note that bacteria are assumed to contact any number of pillars, consistent with experimental observations of bacteria being impaled on one nanopillar. For experiments with capillary forces arising from liquid evaporation, planktonic bacteria contact nanopillars as the water level falls, with positions that are assumed to be random.

References

(1) Mirzaali, M. J.; van Dongen, I. C. P.; Tümer, N.; Weinans, H.; Yavari, S. A.; Zadpoor, A. A. In-silico Quest for Bactericidal but Non-cytotoxic Nanopatterns. *Nanotechnology*, 2018, 29 (43), 43LT02.

(2) Cui, Q.; Liu, T.; Li, X.; Zhao, L.; Wu, Q.; Wang, X.; Song, K.; Ge, D. Validation of the Mechano-bactericidal Mechanism of Nanostructured Surfaces with Finite Element Simulation. *Colloids and Surfaces B: Biointerfaces*, 2021, 206, 111929. DOI: https://doi.org/10.1016/j.colsurfb.2021.111929.

(3) Velic, A.; Hasan, J.; Li, Z.; Yarlagadda, P. Mechanics of Bacterial Interaction and Death on Nanopatterned Surfaces. *Biophysical Journal*, 2021, 120 (2), 217-231.

(4) Islam, M.; Aldawsari, F. S. S.; Yarlagadda, P. K. D. V. Finite Element Modelling of a Gram-Negative Bacterial Cell and Nanospike Array for Cell Rupture Mechanism Study. *Molecules* 2023, *28* (5), 2184.

(5) Valiei, A.; Lin, N.; Bryche, J.-F.; McKay, G.; Canva, M.; Charette, P. G.; Nguyen, D.; Moraes, C.; Tufenkji, N. Hydrophilic Mechano-Bactericidal Nanopillars Require External Forces to Rapidly Kill Bacteria. *Nano Letters*, 2020, 20 (8), 5720-5727.

(6) Valiei, A.; Lin, N.; McKay, G.; Nguyen, D.; Moraes, C.; Hill, R. J.; Tufenkji, N. Surface Wettability Is a Key Feature in the Mechano-Bactericidal Activity of Nanopillars. *ACS Applied Materials & Interfaces*, 2022 (14), 27564–27574.

(7) Wenzel, R. N. Rrsistance of Solid Surfaces to Wetting by Water. *Industrial & Engineering Chemistry*, 1936, 28, 988–994.